This is the peer-reviewed, final accepted version for American Mineralogist, published by the Mineralogical Society of America.
The published version is subject to change. Cite as Authors (Year) Title. American Mineralogist, in press.
DOI: https://doi.org/10.2138/am-2021-7895. http://www.minsocam.org/

# Revision 1

# Lazaraskeite, $Cu(C_2H_3O_3)_2$, the first organic mineral containing glycolate, from the Santa Catalina Mountains, Tucson, Arizona, U.S.A.

Hexiong Yang*[1], Xiangping Gu[2], Ronald B. Gibbs[1], Stanley H. Evans[1], Robert T. Downs[1], and Zak Jibrin[1]

[1]Department of Geosciences, University of Arizona, 1040 E. 4th Street, Tucson, AZ 85721-0077, USA
[2]School of Geosciences and Info-Physics, Central South University, Changsha, Hunan 410083, China

*Corresponding author: hyang@arizona.edu

## Abstract

A new organic mineral species, lazaraskeite, ideally $Cu(C_2H_3O_3)_2$ with two structural forms (designated as form-1 and form-2 hereafter) was discovered in the high elevation of the Santa Catalina Mountains, north of Tucson, Arizona, U.S.A. Both lazaraskeite form-1 and form-2 occur as euhedral individual crystals (up to 0.20 × 0.20 × 0.80 mm) or aggregates, with the former forming more equant crystals and the latter bladed crystals elongated along the *c* axis. Associated minerals include chrysocolla, malachite, wulfenite, mimetite, hydroxylpyromorphite, hematite, microcline, muscovite, and quartz. Both forms of lazaraiskeite are greenish blue in transmitted light, transparent with white streak and vitreous luster. They are brittle and have a Mohs hardness of ~2; cleavage is perfect on {101}. No parting or twinning was observed. The measured and calculated densities are 2.12(2) and 2.138 g/cm$^3$, respectively, for lazaraskeite form-1 and 2.10(2) and 2.086 g/cm$^3$ for lazaraskeite form-2. Optically, lazaraskeite form-1 is biaxial (–), with $\alpha$ =1.595(3), $\beta$ = 1.629(8), $\gamma$ = 1.645(5), $2V_{meas.}$ = 69(2)°, $2V_{cal.}$ = 67°. Lazaraskeite form-2 is also biaxial (–), with $\alpha$ =1.520 (5), $\beta$ = 1.578 (6), $\gamma$ = 1.610 (5), $2V_{meas.}$ = 73(2)°, $2V_{cal.}$ = 70°. Lazaraskeite is insoluble in water or acetone. An electron microprobe analysis for Cu and an Elemental Combustion System equipped with mass spectrometry for C yielded an empirical formula, based on 6 O *apfu*, $Cu_{1.01}(C_{1.99}H_{2.99}O_3)_2$ for lazaraskeite form-1

and $Cu_{1.01}(C_{1.98}H_{3.00}O_3)_2$ for lazaraskeite form-2. The measured $\delta^{13}C$ ‰ values are -37.7(1) and -37.8(1) for lazaraskeite form-1 and form-2, respectively.

Both lazaraskeite form-1 and form-2 are monoclinic with the same space group $P2_1/n$. The unit-cell parameters are $a$ = 5.1049(2), $b$ = 8.6742(4), $c$ = 7.7566(3) Å, $\beta$ = 106.834(2)°, $V$ = 328.75(2) Å$^3$ for form-1 and $a$ = 5.1977(3), $b$ = 7.4338(4), $c$ = 8.8091(4) Å, $\beta$ = 101.418(2)°, $V$ = 333.64(3) Å$^3$ for form-2. Lazaraskeite form-1 is the natural analogue of synthetic bis(glycolato)copper(II), $Cu(C_2H_3O_3)_2$. Its crystal structure is characterized by layers made of octahedrally-coordinated $Cu^{2+}$ cations and glycolate $(C_2H_3O_3)^-$ anionic groups. These layers, parallel to (101), are linked together by the strong hydrogen bonds (O-H…O = 2.58 Å). The $CuO_6$ octahedron is highly distorted, with four equatorial Cu-O bonds between 1.92 and 1.94 Å and two axial bonds at 2.54 Å. Lazaraskeite form-2 has the same topology as lazaraskeite form-2 and possesses all structural features of the low-temperature phase transformed from lazaraskeite form-1 at 220 K (Yoneyama at al. 2013). The major differences between the two structural forms of lazaraskeite include: (1) form-1 has $b > c$, with $\beta$ = 106.8°, whereas form-2 has $b < c$, with $\beta$ = 101.4°; (2) the $CuO_6$ octahedron in form-1 is more elongated and distorted than in form-2; and (3) there is a relative change in the molecular orientation between the two structures.

Lazaraskeite represents the first organic mineral that contains glycolate. Not only does its discovery imply that more glycolate minerals may be found, but also suggests that glycolate minerals may serve as a potential storage for biologically-fixed carbon.

***Key words*:** lazaraskeite, organic mineral, glycolate, crystal structure, X-ray diffraction

## Introduction

The commonly named "organic minerals" include simple and complex salts of different organic acids (such as formic, acetic, citric, mellitic, methanesulfonic and oxalic acids), as well as numerous crystalline hydrocarbons, some amides, imides, porphyrines, triazolate complexes and other compounds (e.g., Mills et al. 2009; Echigo and Kimata 2010). Among minerals derived

from organic acids, oxalates are the most abundant class. In this study, we report a new organic mineral species, lazaraskeite, ideally $Cu(C_2H_3O_3)_2$, found in the high elevation of the mountains just north of Tucson, Arizona, U.S.A. Lazaraskeite possesses two structure forms, which are designated as form-1 and form-2 hereafter for the simplicity of discussion. Lazaraskeite is the first organic mineral that contains glycolate. It is named after its finders, Mr. Warren G. Lazar and Ms. Beverly Raskin Ross. Both Mr. Lazar and Ms. Raskin Ross enjoy prospecting, meteorite and mineral hunting. The new mineral and its name have been approved by the Commission on New Minerals, Nomenclature and Classification (CNMNC) of IMA (IMA 2018-137). Part of the cotype samples have been deposited at the University of Arizona Mineral Museum (Catalogue # 22052 and 22381 for lazaraskeite form-1 and form-2, respectively) and the RRUFF Project (deposition # R180026 and R190015).

Metal-glycolate solids have been an attractive subject of numerous studies. They are mostly prepared as intermediates of chemically and structurally controlled oxide particles (Day et al., 1996; Ksapabutr et al., 2004; Yu et al., 2007; Ng et al., 2008; Das et al., 2009; Pan et al., 2015; Takase et al., 2017, 2018) or metals (Chakroune et al., 2005; Anzlovar et al., 2008; Abdallah et al., 2015, 2018; Takahashi et al., 2016). They have also been investigated as intrinsic functional materials due to their lightness and various physico-chemical properties. For example, their magnetocaloric properties at low temperatures make them valuable for cryogenic magneto-refrigeration applications (Chen et al., 2014) and their chelating properties for an enhanced reactivity in certain catalytic reactions, such as those involved in the polycondensation of ethylene glycol with bis-(hydroxyethyl)terephthalate for the production of poly(ethylene terephthalate) – an important thermoplastic material (Biros et al., 2002). Moreover, because of many coordination possibilities of glycolate molecules (such as bridging, chelating, and terminal modes) (Hubert-Pfalzgraf, 1998), metal-glycolate compounds may exhibit different lattice dimensionalities (zero-, one-, two-, or three-dimensional) formed by metal polyhedra. Thus, structures based on isolated nanoclusters, chains, layers or three-dimensional polymers, including three-dimensional lattices containing shape-controlled cages, can be obtained and their

This is the peer-reviewed, final accepted version for American Mineralogist, published by the Mineralogical Society of America.
The published version is subject to change. Cite as Authors (Year) Title. American Mineralogist, in press.
DOI: https://doi.org/10.2138/am-2021-7895. http://www.minsocam.org/

open structures can be used for gas storages or separations (Abdallah et al. 2018). This paper describes the physical and chemical properties of two forms of lazaraskeite and their crystal structures determined from the single-crystal X-ray diffraction data, demonstrating that lazaraskeite form-1 is the natural analogue of synthetic bis(glycolate)copper(II) $Cu(C_2H_3O_3)_2$ (e.g., Prout et al. 1968; Ye et al. 2010; Yoneyama et al. 2013, 2016) and lazaraskeite form-2 the low-temperature phase of lazaraskeite form-1 below 220 K (Yoneyama et al. 2013).

## Sample Description and Experimental Methods

*Occurrence, physical and chemical properties, and Raman spectra*

Both lazaraskeite form-1 and form-2 were found on the western end of Pusch Ridge in the high elevation (975 m) of the Santa Catalina Mountains (32° 21′ 42″ N, 110° 57′ 30″ W), north of Tucson, Pima County, Arizona, USA. They occur in a heavily fractured leucogranite, 3 to 5 feet below the rock surface (Figure 1), with lazaraskeite form-2 found in the relatively deeper area. Crystals of lazaraskeite form-1 and form-2 occur as individuals (up to 0.20 x 0.20 x 0.80 mm) or aggregates, but the former usually are found with a more equant morphology, and the latter as bladed crystals elongated along the *c* axis (Figure 2). Associated minerals include chrysocolla, malachite, wulfenite, mimetite, hydroxylpyromorphite, hematite, microcline, muscovite, and quartz. Lazaraskeite is a secondary mineral believed to have formed through the interaction of fluids containing glycolic acid ($C_2H_4O_3$) with copper produced by the oxidation of primary and secondary minerals.

Both lazaraskeite form-1 and form-2 are greenish blue in transmitted light, transparent with white streak and vitreous luster, but crystals of lazaraskeite form-2 appear to be relatively more pale-blue than those of lazaraskeite form-1. They are brittle and have a Mohs hardness of ~2; cleavage is perfect on {101}. No parting or twinning was observed. The measured (by flotation in heavy liquids) and calculated densities for the two forms are given in Table 1. Optically, lazaraskeite form-1 is biaxial (–), with $\alpha$ =1.595(3), $\beta$ = 1.629(8), $\gamma$ = 1.645(5), $2V_{meas.}$ = 69(2)°, $2V_{cal.}$ = 67°, and the orientation $X \wedge c = 42°$, $Y = b$. The pleochroism is $X = Z$ = light blue

green and *Y* = blue green, and the dispersion v > r (weak). Lazaraskeite form-2 is also biaxial (–), with $\alpha$ =1.520 (5), $\beta$ = 1.578 (6), $\gamma$ = 1.610 (5), $2V_{meas.}$ = 73(2)°, $2V_{cal.}$ = 70° and the orientation *X* ^*c* = 36°, *Y* = *b*. The pleochroism is *X* = *Z* = pale blue and *Y* = greenish blue, and the dispersion v > r (weak). Lazaraskeite is insoluble in water or acetone. The compatibility indices for the two forms were not calculated because of the lack in a *k*-value for the glycolate group.

The chemical compositions of lazaraskeite form-1 and form-2 were determined using a CAMECA SX-100 electron microprobe (WDS mode, 10 kV, 6 nA, and 5 μm beam diameter, 2s counting) for Cu and an Elemental Combustion System equipped with mass spectrometry for C (Table 2), as well as $\delta^{13}$C ‰. The resultant empirical chemical formula, calculated on the basis of 6 O *apfu* (from the structure determination), is $Cu_{1.01}(C_{1.99}H_{2.99}O_3)_2$ for lazaraskeite form-1 and $Cu_{1.01}(C_{1.98}H_{3.00}O_3)_2$ for lazaraskeite form-2, both of which can be simplified to $Cu(C_2H_3O_3)_2$. The measured $\delta^{13}$C ‰ values are -37.7(1) and -37.8(1) for lazaraskeite form-1 and form-2, respectively. According to O'Leary (1988), such a value would result from C3-type plants with limiting carboxylation but fast diffusion. The predicted $\delta^{13}$C ‰ value for such plants is -38. For the comparison, we also measured the $\delta^{13}$C ‰ value from the roots that were intimately associated with lazaraskeite, which is -23.4(1), consistent with $\delta^{13}C_{VPDB}$ ‰ values of −20 to −37‰ for C3-type plants (Kohn 2010).

The Raman spectra of two lazaraskeite forms were collected from randomly oriented crystals on a Thermo Almega microRaman system, using a solid-state laser with a frequency of 532 nm and a thermoelectric cooled CCD detector. The laser is partially polarized with 4 $cm^{-1}$ resolution and a spot size of 1 μm.

*X-ray crystallography*

The X-ray powder diffraction data of lazaraskeite were collected with a Rigaku D/Max 2500 diffractometer using Cu*K*α radiation (Table 3). Unit cell parameters refined from the powder data are *a* = 5.1041(4), *b* = 8.6705(8), *c* =7.7508(6) Å, β = 106.747(5)º, and *V* =

This is the peer-reviewed, final accepted version for American Mineralogist, published by the Mineralogical Society of America.
The published version is subject to change. Cite as Authors (Year) Title. American Mineralogist, in press.
DOI: https://doi.org/10.2138/am-2021-7895. http://www.minsocam.org/

328.46(3) Å$^3$ for lazaraskeite form-1, and $a$ = 5.1916 (2), $b$ = 7.4048 (4), $c$ = 8.8036 (5) Å, β = 101.462 (4)º, and $V$ = 331.69 (1) Å$^3$ for lazaraskeite form-2.

Single-crystal X-ray diffraction data for lazaraskeite were collected on a Bruker X8 APEX2 CCD X-ray diffractometer equipped with graphite-monochromatized Mo$K_\alpha$ radiation from nearly equidimensional crystals (0.05 x 0.04 x 0.04 mm for lazaraskeite form-1 and 0.06 x 0.06 x 0.05 mm for lazaraskeite form-2) with frame widths of 0.5° in ω and 30 s counting time per frame. All reflections for two forms of lazaraiskeite were indexed on the basis of a monoclinic unit-cell (Table 1). The intensity data were corrected for X-ray absorption using the Bruker program SADABS. The systematic absences of reflections suggest the unique space group $P2_1/n$ for both forms. Their structures were solved and refined using SHELX2018 (Sheldrick 2015a, 2015b). All H atoms were located from the difference Fourier maps. The ideal chemistry was assumed during the refinements. The positions of all atoms were refined with anisotropic displacement parameters, except those for the H atoms, which were refined only with isotropic parameters. Final coordinates and displacement parameters of atoms in lazaraskeite are listed in cif (supplemental material), and selected bond-distances in Table 4.

## Discussion

### *Crystal structures*

Lazaraskeite form-1 is the natural analogue of synthetic bis(glycolato)copper(II), $Cu(C_2H_3O_3)_2$, which has been extensively studied for both its scientific and industrial interests (e.g., Prout et al. 1968; Ye et al. 2010; Yoneyama et al. 2013, 2016). Its crystal structure is characterized by layers of $Cu^{2+}$ cations that are octahedrally coordinated to glycolate $(C_2H_3O_3)^-$ anionic groups (Figures 3 and 4). These layers are parallel to (101), accounting for the perfect cleavage of the mineral, and are linked together by the relatively strong hydrogen bonding (O2-H1…O3 = 2.58 Å) (Figure 5). Due to the Jahn-Teller effect, the $CuO_6$ octahedron is highly distorted, with four equatorial Cu-O bonds between 1.92 and 1.94 Å and two axial bonds at 2.54 Å.

This is the peer-reviewed, final accepted version for American Mineralogist, published by the Mineralogical Society of America.
The published version is subject to change. Cite as Authors (Year) Title. American Mineralogist, in press.
DOI: https://doi.org/10.2138/am-2021-7895. http://www.minsocam.org/

Lazaraskeite form-2 has the same topology as lazaraskeite form-1 (Figures 3, 4, and 5). However, the two forms also exhibit some noticeable structural differences. For example, lazaraskeite form-1 has $b > c$, with $\beta = 106.8°$, whereas lazaraskeite form-2 has $b < c$, with $\beta = 101.4°$ (Table 1). Moreover, the $CuO_6$ octahedron in lazaraskeite form-1 is more elongated than that in lazaraskeite form-2 (2.54 vs. 2.44 Å for the axial Cu-O bonds) (Table 4). There is also a relative change in the molecular orientation between the two structures, as shown in Figures 3 and 4.

By means of both single-crystal X-ray diffraction and magnetic measurements, Yoneyama et al. (2013) observed an isosymmetric structural transformation [or so-called "type 0" transition according to Christy (1995)] of synthetic lazaraskeite form-1 at 220 K to a low-temperature phase. This phase transition, which is reversible and shows a large hysteresis (220-270 K), is marked by a discontinuous change in the paramagnetic susceptibility, unit-cell parameters (from $b > c$ to $c > b$), and axial Cu-O bonds in the elongated $CuO_6$ octahedra (from 2.54 to 2.44 Å). Isosymmetric structural phase transitions have been observed in a number of compounds, such as $(Mg_{0.75}Fe_{0.25})_2Si_2O_6$ orthopyroxene (Yang and Ghose 1995), $C_{13}H_{22}N^+ \cdot ClO_4^-$ (Wu and Jin 2013), and $LaGaO_3$ (Tang et al. 2018). Remarkably, the crystal structure of the low-temperature phase of lazaraskeite form-1 at 150 K determined by Yoneyama et al. (2013) is identical to that of lazaraskeite form-2 if the thermal effects due to the temperature difference are taken into account (Tables 1 and 4). Nonetheless, it is unclear why the two structure forms of lazaraskeite can occur in the same place. The chemical analyses on two form crystals did not detect other elements except Cu and C. Perhaps, the different Eh or/and pH environments might play a role, as lazaraskeite form-2 was found in a relatively deeper place (below 5 feet) than lazaraskeite form-1. The obvious difference in crystal morphologies of two forms appears to rule out the possibility that one structure form was transformed directly from the other. Interestingly, the co-existence of two polymorphs with the same symmetry and similar unit-cell parameters has been reported for the Cu-bearing organic compound $(\alpha\text{-pic})_2Cu(NO_3)_2$ (α-pic = 2-methylpyridine) (Cameron et al. 1972). Both forms of this material are monoclinic,

190 space group $P2_1/c$, with unit-cell parameters $a$ = 8.31, $b$ = 14.81, $c$ = 14.14 Å, β = 123.9° (Form
191 I) and $a$ = 8.57, $b$ = 14.39, $c$ = 14.20 Å, β = 119.5° (Form II).
192
193 *Raman spectra*
194 The Raman spectra of the two forms of lazaraskeite are shown in Figure 6. The strong
195 resemblance between the two spectra is expected, as the structures of the two forms are similar.
196 The difference in peak intensities between the two spectra principally results from the different
197 crystal orientations when the data were collected. The tentative assignments of major Raman
198 bands were made (Table 5) based on both experimental and theoretical spectroscopic studies on
199 synthetic compounds containing the glycolic group $(C_2H_3O_3)^-$ (e.g., Medina et al. 2001; Silva et
200 al. 2013; Gomes et al. 2014; do Nascimento et al. 2017). In particular, the bands between 1200-
201 1670 $cm^{-1}$ are attributed to the C-O and C-C stretching vibrations in the $C_2H_3O_3^-$ glycolic group
202 and those from 840 to 1100 $cm^{-1}$ to the C-OH stretching vibrations, as well as the O-C-O
203 bending vibrations in $C_2H_3O_3^-$ glycolic group.
204
205 *Sources of glycolate*
206 Many plants are known to produce glycolate during photorespirations in reactions
207 catalyzed by glycolate oxidase or isocitrate lyase (Igamberdiev and Eprintsev 2016; Claassens et
208 al. 2020 and references therein). However, whether such glycolate produced within plants can
209 become available directly to form lazaraskeite in rocks several feet below the surface is
210 unknown. Nevertheless, root exudates of many plants consist of a complex mixture of organic
211 acid anions (including glycolic), phytosiderophores, sugars, vitamins, amino acids, purines,
212 nucleosides, inorganic ions (e.g. $HCO_3^-$, $OH^-$, $H^+$), gaseous molecules ($CO_2$, $H_2$), and enzymes
213 (e.g., Dakora and Phillips 2002; Engqvist et al. 2015). Plants take up most mineral nutrients
214 through the rhizosphere where root exudates interact with microorganisms in soils and rocks.
215 Thus, a possible formation mechanism for lazaraskeite occurs when plant root exudates

containing glycolic acid encounter Cu-bearing minerals, such as chrysocolla, $(Cu_{2-x}Al_x)H_{2-x}Si_2O_5(OH)_4 \cdot nH_2O$, and malachite, $Cu_2(CO_3)(OH)_2$.

Numerous studies have demonstrated that glycolate can also be produced through the biodegradation of a number of organic matters by microorganisms under aerobic conditions (e.g., van Ginkel 1996; Liu et al. 2018; Fujiwara et al. 2020). In particular, Hunkeler and Aravera (2000) showed that glycolate is generated during the metabolic pathway of 1,2-dichloroethane (DCA) degradation (from ethane → ethanol → glycolate → glyoxylate) by the aerobic bacterium *Xanthobacter autotrophicus* **GJ10**. Furthermore, they found that this degradation process is accompanied by a strong carbon isotope fractionation, with the produced inorganic carbon depleted significantly in $^{13}C$ ($\delta^{13}C$ = -46.2‰) and the biomass enriched in $^{13}C$ ($\delta^{13}C$ = -17.2‰), as compared to the initially added 1,2-DCA ($\delta^{13}C$ = -30.6‰). If we assume that aerobic microbial degradation of root exudates was involved in the formation of lazaraskeite, then, the observation by Hunkeler and Aravera (2000) may render an explanation for the $\delta^{13}C$ value of -37.7‰ we measured for lazaraskeite,

Some microorganisms are also capable of producing glycolate (e.g., Burnap et al. 2015; Dellero et al. 2016; Taubert et al. 2019). For example, according to Eisenhut et al. (2008), the cyanobacterium *Synechocystis* has established three different routes for the metabolism of glycolate. One is similar to the bacterial glycolate metabolism, the second resembles the photorespiratory cycle found in higher plants, and the third involves the complete oxidation of glycolate to $CO_2$. As microorganisms are ubiquitous in nature, their contributions as a potential glycolate source for the formation of lazaraskeite should not be excluded.

Glycolate can be converted from oxalate, or vice versa, through the redox reactions either biotically or abiotically. In human bodies, the conversion between glycolate and oxalate is intimately associated with obesity and subsequent development of chronic diseases, as well as the formation of kidney stones (Knight et al. 2010). The conversion between glycolate and oxalate in metabolic pathways of plants is the key to the accumulations of biologically-fixed carbon (Igamberdiev and Eprintsev 2016). Recently, the abiotic transition between glycolate and

243 oxalate as a redox couple has attracted considerable attention because it demonstrates a carbon-
244 neutral or $CO_2$-free energy circulation with the help of some metals or oxides as catalysts
245 (Fukushima et al. 2018 and references therein). In Arizona, several oxalate minerals, such as
246 weddellite ($CaC_2O_4 \cdot 2H_2O$), whewellite ($CaC_2O_4 \cdot H_2O$), and glushinskite ($MgC_2O_4 \cdot 2H_2O$), are
247 abundant in decaying plants, especially cacti (e.g., Franceschi and Horner 1980; Horner and
248 Wagner 1995; Prychid and Rudall 1999; Garvie 2003). These oxalate minerals are formed from
249 elements released from the decaying plants by microorganisms. The $\delta^{13}C_{VPDB}$ values of the
250 monohydrocalcite and calcite transformed from weddellite in the decaying Saguaro Cactus range
251 from –1.65 to + 0.76‰, indicating that the carbon in weddellite was derived from atmospheric
252 $CO_2$ (Garvie 2003). Accordingly, the possibility for oxalate in these minerals to be eventually
253 converted abiotically to glycolate in lazaraskeite can be precluded, as the $\delta^{13}C_{VPDB}$ value we
254 measured for lazaraskeite is -37.7‰.
255
256 **Implications**
257 A great number of glycolate compounds containing $M^{n+}$ cations (n = 1, 2, 3, or 4) have
258 been synthesized in laboratories, including lazaraskeite form-1, $Ni(C_2H_3O_3)_2$, $Co(C_2H_3O_3)_2$, and
259 $[Mg(C_2H_3O_3)(H_2O)_4]NO_3$ (e.g., Prout et al. 1968; Medina et al. 2000; Melikyan et al. 2000;
260 Kang et al. 2004; Ye et al. 2010; Liu et al. 2011; Lin et al. 2013; Silva et al. 2013; Yoneyama et
261 al. 2013; Gomes et al. 2014; Song and Hirato 2015; do Nascimento et al. 2017; Abdallah et al.
262 2018). In nature, glycolic acid ($C_2H_4O_3$) is a common and abundant organic matter that can be
263 generated from several biological sources (see above). It is a product of fixed carbon
264 accumulated in the conversion process of carbon compounds in metabolic pathways. The
265 discovery of lazaraskeite, therefore, not only leads to the postulation that more glycolate
266 minerals may be found, but also implies that glycolate minerals may serve as a potential storage
267 for biologically-fixed carbon. Because glycolate is more stable in the reduced environments than
268 oxalate, which usually forms various minerals on the ground surface or in decaying plants, we
269 would expect more glycolate minerals, like lazaraskeite, to be found from the subsurface.

This is the peer-reviewed, final accepted version for American Mineralogist, published by the Mineralogical Society of America.
The published version is subject to change. Cite as Authors (Year) Title. American Mineralogist, in press.
DOI: https://doi.org/10.2138/am-2021-7895. http://www.minsocam.org/

In addition to lazaraskeite form-1 and lazaraskeite form-2, the compound $Cu(C_2H_3O_3)_2$ appears to have another polymorph (designated as phase A for the simplicity of discussion) (Lin et al. 2013), which is dark blue in color and monoclinic with the same space group ($P2_1/n$) as lazaraskeite, but has a unit-cell volume twice that of lazaraskeite. The crystal structure of phase A exhibits many features similar to those in lazaraskeite, such as the coordination environments around $Cu^{2+}$ cations and the layers formed by $Cu^{2+}$ and $(C_2H_3O_3)^-$, which are linked together by hydrogen bonds. However, the $CuO_6$ octahedron in phase A is the most distorted and elongated of all three forms, with one axial Cu-O bond at 2.843 Å and the other at 2.642 Å. Compared to synthetic lazaraskeite form-1, which can be obtained with solution reactions between 60-80 °C (Ye et al. 2010; Yoneyama et al. 2013), phase A was synthesized at a much higher temperature (120 °C) (Lin et al. 2013). Because lazaraskeite form-1 transforms to lazaraskeite form-2 at low temperature (Yoneyama et al. 2013), which is characterized by a significant shortening of the axial Cu-O bonds in the $CuO_6$ octahedron, it then begs the question whether phase A can be attained by heating lazaraskeite form-1, as the axial Cu-O bonds in phase are markedly longer than those in lazaraskeite form-1.

Synthetic glycolate compounds $Ni(C_2H_3O_3)_2$ and $Co(C_2H_3O_3)_2$ have been regarded isostructural with lazaraskeite form-1 (e.g., Medina et al. 2000; Kang et al. 2004; Nakane et al. 2019, 2020). However, a detailed structural comparison reveals that the $NiO_6$ and $CoO_6$ octahedra in $Ni(C_2H_3O_3)_2$ and $Co(C_2H_3O_3)_2$, respectively, are much less distorted than the $CuO_6$ octahedra in lazaraskeite form-1, with all Ni-O bonds between 2.00 and 2.10 Å (Kang et al. 2004; Nakane et al. 2020) and Co-O bonds between 2.05 and 2.12 Å (Medina et al. 2000; Nakane et al. 2019). Moreover, the relative orientations between $NiO_6/CoO_6$ octahedra and glycolic groups in $Ni(C_2H_3O_3)_2$ and $Co(C_2H_3O_3)_2$ are more similar to those in lazaraskeite form-2, rather than in lazaraskeite form-1. Given these structural features, together with the fact that, like lazaraskeite form-2, both $Ni(C_2H_3O_3)_2$ and $Co(C_2H_3O_3)_2$ have the unit-cell parameters $c > b$ (Medina et al. 2000; Kang et al. 2004; Nakane et al. 2019, 2020), not $b > c$ (like those for lazaraskeite form-1), we suggest that these two Ni and Co compounds are better considered as

297 analogues of lazaraskeite form-2, instead of lazaraskeite form-1. This consideration may also
298 provide an explanation (at least in part) as to why no structural transformation was observed for
299 $Ni(C_2H_3O_3)_2$ between 299 and 96 K (Nakane et al. 2020) or $Co(C_2H_3O_3)_2$ between 298 and 5 K
300 (Nakane et al. 2019), in contrast to lazaraskeite form-1, which undergoes a first-order phase
301 transformation to lazaraskeite form-2 at 220 K (Yoneyama et al. 2013).
302

303 **Acknowledgements**

304 This study was supported partially by Mr. Michael M. Scott.
305

306 **References Cited**

307 Abdallah, A., Gaudisson, T., Sibille, R., Nowak, S., Cheikhrouhou-Koubaa, W., Shinoda, K.,
308 Francois, M., and Ammar, S. (2015) Structural and magnetic properties of mixed Co-Ln
309 (Ln = Nd, Sm, Eu, Gd and Ho) diethyleneglycolate complexes. Dalton Transactions, 44,
310 16013-16023.
311 Abdallah, A., Ammar, S., Ban, V., Sibille, R., and Francois, M. (2018) Ab initio structure
312 determination of $[Eu_5(C_2H_4O_2)_6(CH_3CO_2)_3]_n$ by X-ray powder diffraction. Acta
313 Crystallographica, B74, 592-597.
314 Anzlovar, A., Orel, Z.C., and Zigon, M. (2008) Morphology and Particle Size of Di(ethylene
315 glycol) Mediated Metallic Copper Nanoparticles. Journal of Nanoscience and
316 Nanotechnology, 8, 3516-3525.
317 Biros, S.M., Bridgewater, B.M., Villeges-Estrada, A., Tanski, J.M., and Parkin, G. (2002)
318 Antimony ethylene glycolate and catecholate compounds: Structural characterization of
319 polyesterification catalysts. Inorganic Chemistry, 41, 4051-4057.
320 Burnap, R.L., Hagemann, M., and Kaplan, A. (2015) Regulation of $CO_2$ concentrating
321 mechanism in cyanobacteria. Life, 5, 348–371.
322 Cameron, A.F., Taylor, D.W., and Nuttall, R.H. (1972) Structural investigations of metal nitrate
323 Complexes. Part III. Crystal and molecular structures of two crystalline forms of

dinitratobis( α-picoline)copper(II). Dalton Transactions, 58-63.

Chakroune, N., Viau, G., Ammar, S., Jouini, N., Gredin, P., Vaulay, M.J., and Fievet, F. (2005) Synthesis, characterization and magnetic properties of disk-shaped particles of a cobalt alkoxide: Co-II($C_2H_4O_2$). New Journal of Chemistry, 29, 355-361.

Chen, Y.C., Guo, F.S., Liu, J.L., Leng, J.D., Vrabel, P., Orendac, M., Prokleska, J., Sechovsky, V., and Tong, M.L. (2014) Switching of the Magnetocaloric Effect of Mn-II Glycolate by Water Molecules. Chemistry-A European Journal, 20, 3029-3035.

Christy, A.G. (1995) Isosymmetric Structural Phase Transitions: Phenomenology and Examples. Acta Crystallographica, B51, 753-757.

Claassens, N.J., Scarinci, G., Fischer, A., Flamholz, A.I., Newell, W., Frielingsdorf, S., Lenz, O., and Bar-Even, A. (2020) Phosphoglycolate salvage in a chemolithoautotroph using the Calvin cycle. Proceedings of the National Academy of Sciences of the United States of America, 117, 22452-22461.

Dakora, F.D. and Phillips, D.A. (2002) Root exudates as mediators of mineral acquisition in low-nutrient environments. Plant and Soil, 245, 35-47.

Das, J., Evans, I.R., and Khushalani, D. (2009) Zinc Glycolate: A Precursor to ZnO. Inorganic Chemistry, 48, 3508-3510.

Day, V.W., Eberspacher, T.A., Frey, M.H., Klemperer, W.G., Liang, S., and Payne, D.A. (1996) Barium titanium glycolate: A new barium titanate powder precursor. Chemistry of Materials, 8, 330-332.

Dellero, Y., Jossier, M., Schmitz, J., Maurino, V.G., and Hodges, M. (2016) Photorespiratory glycolate–glyoxylate metabolism. Journal of Experimental Botany, 67, 3041–3052.

do Nascimento, A.L.C.S., Teixeira1, J.A., Nunes, W.D.G., Gomes, D.J.C., Gaglieri, C., Treu-Filho, O., Pivatto, M., Caires, F.J., and Ionashiro, M. (2017) Thermal behavior of glycolic acid, sodium glycolate and its compounds with some bivalent transition metal ions in the solid state. Journal of Thermal Analysis and Calorimetry, 130, 1463–1472.

Echigo, T. and Kimata, M. (2010) Crystal chemistry and genesis of organic minerals: a review of

oxalate and polycyclic aromatic hydrocarbon minerals. The Canadian Mineralogist, 48, 1329-1358.

Eisenhut, M., Ruth, W., Haimovich, M., Bauwe, H., Kaplan, A., and Hagemann, M. (2008). The photorespiratory glycolate metabolism is essential for cyanobacteria and might have been conveyed endosymbiontically to plants. Proceedings of the National Academy of Sciences of the United States of America, 105, 17199–17204.

Engqvist, M.K.M., Schmitz, J., Gertzmann, A., Florian, A., Jaspert, N., Arif, M., Balazadeh, S., Mueller-Roeber, B., Fernie, A.R., and Maurino. V.G. (2015) Glycolate oxidase3, a glycolate oxidase homolog of yeast L-lactate cytochrome c oxidoreductase, supports L-lactate oxidation in roots of Arabidopsis. Plant Physiology, 169, 1042-1061.

Franceschi, V.R. and Horner, H.T., Jr. (1980) Calcium oxalate crystals in plants. Botanical Reviews, 46, 361–427.

Fukushima, T., Kitano, S., Hata, S., and Yamauchi, M. (2018) Carbon-neutral energy cycles using alcohols. Science and Technology of Advanced Materials, 19, 142-152.

Fujiwara, R., Noda, S., Tanaka, T., and Kondo, A. (2020) Metabolic engineering of *Escherichia coli* for shikimate pathway derivative production from glucose–xylose co-substrate. Nature Communications**, 11,** 279. https://doi.org/10.1038/s41467-019-14024-1.

Garvie, L.A.J. (2003) Decay-induced biomineralization of the saguaro cactus (Carnegiea gigantea). American Mineralogist, 88, 1879-1888.

Gomes, D.J.C., Caires, F.J., Silva, R.C., Treu-Filho, O., and Ionashiro, M. (2014) Synthesis, characterization, thermal and spectroscopic studies of solidglycolate of light trivalent lanthanides, except promethium. Thermochimica Acta, 587, 33–41.

Horner, H.T. and Wagner, B.L. (1995) Calcium oxalate formation in higher plants. In S.R. Khan, Ed., Calcium Oxalate in Biological Systems, p. 53–72, CRC Press, Florida.

Hubert-Pfalzgraf, L.G. (1998) Some aspects of home and heterometallic alkoxides based on functional alcohols. Coordination Chemistry Reviews, 178, 967-997.

Hunkeler, D. and Aravera, R. (2000) Evidence of Substantial Carbon Isotope Fractionation

among Substrate, Inorganic Carbon, and Biomass during Aerobic Mineralization of 1,2-Dichloroethane by Xanthobacter autotrophicus. Applied and Environmental Microbiology, 66, 4870–4876.

Igamberdiev, A.U. and Eprintsev, A.T. (2016) Organic Acids: The Pools of Fixed Carbon Involved in Redox Regulation and Energy Balance in Higher Plants. Frontiers in Plant Science, 7, 1-15.

Kang, Q-Q., Long, L-S., Huang, R-B., and Zheng, L-S. (2004) Polymeric bis(glycolato)nickel(II). Acta Crystallographica, E60, 406-407.

Knight, J. Assimos, D.G., Easter, L., and Holmes, R.P. (2010) Metabolism of Fructose to Oxalate and Glycolate. Hormone and Metabolic Research, 42, 868–873.

Kohn, M.J. (2010) Carbon isotope compositions of terrestrial C3 plants as indicators of (paleo)ecology and (paleo)climate. Proceedings of the National Academy of Sciences of the United States of America, 107, 19691-19695.

Ksapabutr, B., Gulari, E., and Wongkasemjit, S. (2004) One-pot synthesis and characterization of novel sodium tris(glycozirconate) and cerium glycolate precursors and their pyrolysis. Materials Chemistry and Physics, 83, 34-42.

Lin, X.S., Sang, Y.L., Sun, W.D., and Yang, S.H. (2013) Assembly of three coordination polymers from glycolate ligands: syntheses, crystal structures, and thermal properties. Transition Metal Chemistry, 38, 503–509.

Liu, W., Wei, Z., and Yue, S. (2011) Tetraaqua(2-hydroxyacetato-$\kappa^2$ $O^1$,$O^2$)-magnesium nitrate. Acta Crystallographica, E67, m374.

Liu, M., Ding, Y., Xian, M., and Zhao, G. (2018) Metabolic engineering of a xylose pathway for biotechnological production of glycolate in *Escherichia coli*. Microbial Cell Factories, 17, 51 (1-11).

Medina, G., Gasque, L., and Bernés, S. (2000) Polymeric bis(glycolato)cobalt(II). Acta Crystallographica, C56**,** 637-638.

Medina, G., Bernès, S., Martínez, A., and Gasque, L. (2001) Infrared assignment of

bis(glycolato)-bis(pyridine) metal(ii) compounds and crystal structure of *trans*bis(glycolato)-*cis*-bis(pyridine)nickel(ii) dihydrate. Journal of Coordination Chemistry, 54, 267-284.

Melikyan, G.G., Amiryan, F., Visi, M., Hardcastle, K.I., Bales, B.L., Aslanyan, G., and Badanyan, S.H. (2000) Manganese(II):(III) glycolates: preparation, X-ray crystallographic study, and application in radical cycloaddition reactions. Inorganica Chimica Acta, 308, 45–50.

Mills, S.J., Hatert, F., Nickel, E.H., and Ferraris, G. (2009): The standardisation of mineral group hierarchies: application to recent nomenclature proposals. European Journal of Mineralogy, 21, 1073-1080.

Nakane, T., Yoneyama, S., Kodama, T., Kikuchi, K., Nakao, A., Ohhara, T., Higashinaka, R., Matsuda, T.D., Aokie, Y., and Fujita, W. (2019) Magnetic, thermal, and neutron diffraction studies of a coordination polymer: bis(glycolato)cobalt(II). Dalton Transactions, 48, 333–338.

Nakane, T., Aoyagia, S., and Fujita, W. (2020) Magnetic and thermal studies of a coordination polymer: bis(glycolato)nickel(II). New Journal of Chemistry, 44, 10519-10524.

Ng, S.H., Chew, S.Y., Santos, D.I., Chen, J., Wang, J.Z., Dou, S.X., and Liu, H.K. (2008) Hexagonal-shaped tin glycolate particles: A preliminary study of their suitability as li-ion insertion electrodes. Chemistry-An Asian Journal, 3, 854-861.

O'Leary, M.H. (1988) Carbon isotopes in photosynthesis. BioScience, 38, 328-336.

Pan, G.H., Hayakawa, T., Nogami, M., Hao, Z., Zhang, X., Qu, X., and Zhang, J.H. (2015) Zinc titanium glycolate acetate hydrate and its transformation to zinc titanate microrods: synthesis, characterization and photocatalytic properties. RSC Advances, 5, 88590-88601.

Prout, C.K., Armstrong, R.A., Carruthers, J.R., Forrest, J.G., Murray-Rust, P., and Rossotti, F.J.C. (1968) Structure and stability of carboxylate complexes. Part I. The crystal and molecular structures of copper(II) glycolate, DL-lactate, 2-hydroxy-2-methylpropionate,

methoxyacetate, and phenoxyacetate, Journal of Chemical Society (A), 1968, 2791-2813.

Prychid, C.J. and Rudall, P.J. (1999) Calcium oxalate crystals in Monocotyledons: A review of their structure and systematics. Annals of Botany, 84, 725–739.

Sheldrick, G. M. (2015a) SHELXT – Integrated space-group and crystal structure determination. Acta Crystallographica, A71, 3-8.

Sheldrick, G. M. (2015b) Crystal structure refinement with SHELX. Acta Crystallographica, C71, 3-8.

Silva, R.C., Caires, F.J., Gomes, D.J.C., Gigante, A.C., and Ionashiro, M. (2013) Synthesis, characterization and thermal studies of alkaline earth glycolate, except beryllium and radium. Thermochimica Acta, 573, 170– 174.

Song, D. and Hirato, T. (2015) Fabrication of Three-Dimensional Titania Building Blocks on Glass Substrate from Mono-Dispersed Titanium Glycolate Spheres and Their Photocatalystic Properties. Materials Transactions, 56, 348-352.

Takahashi, K., Yokoyama, S., Matsumoto, T., Huaman, J.L.C., Kaneko, H., Piquemal, J-Y., Miyamura, H., and Balachandran, J. (2016) Towards a designed synthesis of metallic nanoparticles in polyols - elucidation of the redox scheme in a cobalt-ethylene glycol system. New Journal of Chemistry, 40, 8632-8642.

Takase, K., Nishizawa, H., Onda, A., Yanagisawa, K., and Yin, S. (2017) Synthesis and characterization of glycolate precursors to $MTiO_3$ ($M = Ni^{2+}$, $Co^{2+}$, $Zn^{2+}$). Journal of Asian Ceramic Society, 5, 482-488.

Takase, K., Nishizawa, H., Imamura, K., Onda, A., Yanagisawa, K., and Yin, S. (2018) Synthesis of Novel Layered Zinc Glycolate and Exchange of Ethylene Glycol with Manganese Acetate Complex. Bulletin of the Chemical Society of Japan, 91, 1546-1552.

Tang, Y.Q., López-Cartes, C., Avilés, M.A., and Córdoba, J.M. (2018) Isosymmetric structural phase transition of the orthorhombic lanthanum gallate structure as a function of temperature determined by Rietveld analysis. CrystEngComm**,** 20, 5562-5569.

Taubert, A., Jakob, T., and Wilhelm, C. (2019) Glycolate from microalgae: an efficient carbon

source for biotechnological applications. Plant Biotechnology Journal, 1-9.

van Ginkel, C.G. (1996) Complete degradation of xenobiotic surfactants by consortia of aerobic microorganisms. Biodegradation, 7, 151–164.

Wu, D-H. and Jin, L. (2013) Temperature-induced isosymmetric reversible structural phase transition in triethylbenzylammonium perchlorate. Inorganic Chemistry Communications, 29, 151-156.

Yang, H. and Ghose, S. (1995) A transitional structural state and anomalous Fe-Mg order-disorder in Mg-rich orthopyroxene, $(Mg_{0.75}Fe_{0.25})_2Si_2O_6$. American Mineralogist, 80, 9-20.

Ye, Q-S., Xie, M-J., Liu, W-P., Chen, X-Z., Chang, Q-W., and Yu, Y. (2010) Refinement of the crystal structure of bis(glycolato)copper(II), $Cu(C_2H_3O_3)_2$. Zeitschrift für Kristallographie, 225, 481-482.

Yoneyama, S., Kodama, T., Kikuchi, K., Kawabata, Y., Kikuchi, K., Ono, T., Hosokoshi, Y., and Fujita, W. (2013) Large structural transformation and ferromagnetic ordering in a coordination polymer with a two-dimensional square-planar lattice, bis(glycolato)copper(II). CrystEngComm, 15, 10193–10196.

Yoneyama, S., Kodama, T., Kikuchi, K., Fujisawa, T., Yamaguchi, A., Sumiyama, A., Shuku, Y., Aoyagi, S., and Fujita, W. (2016) Deuterium substitution effects on the structural and magnetic phase transitions of a hydrogen-bonded coordination polymer, bis(glycolato)copper(II). Dalton Transactions, 45, 16774–16778.

Yu, H.K., Eun, T.H., Yi, G.R., and Yang, S.M. (2007) Multi-faceted titanium glycolate and titania structures from room-temperature polyol process. Journal of Colloid and Interface Science, 316, 175-182.

## List of Tables



## List of Figure Captions

Table 1. Comparison of crystallographic data between lazaraskeite-$M_1$ and lazaraskeite-$M_2$

| | lazaraskeite-$M_1$ | Synthetic | lazaraskeite-$M_2$ | Synthetic, at 150K |
|---|---|---|---|---|
| Ideal chemical formula | $Cu(C_2H_3O_3)_2$ | $Cu(C_2H_3O_3)_2$ | $Cu(C_2H_3O_3)_2$ | $Cu(C_2H_3O_3)_2$ |
| Crystal symmetry | Monoclinic | Monoclinic | Monoclinic | Monoclinic |
| Space group | $P2_1/n$ | $P2_1/n$ | $P2_1/n$ | $P2_1/n$ |
| $a$ (Å) | 5.1049(2) | 5.1095(9) | 5.1977(3) | 5.178(4) |
| $b$ (Å) | 8.6742(4) | 8.677(2) | 7.4338(4) | 7.208(5) |
| $c$ (Å) | 7.7566(3) | 7.746(1) | 8.8091(4) | 8.889(7) |
| $\beta$ (°) | 106.834(2) | 106.841(2) | 101.418(2) | 100.840(9) |
| $V$(Å$^3$) | 328.75(2) | 328.7 | 333.64(3) | 325.8(5) |
| | | | | |
| $a$:$b$:$c$ | **0.59 : 1 : 0.89** | **0.60 : 1 : 0.89** | **0.70 : 1 : 1.19** | **0.72 : 1 : 1.23** |
| Z | 2 | 2 | 2 | 2 |
| $\rho_{meas}$(g/cm$^3$) | 2.12(2) | | 2.10(2) | |
| $\rho_{cal}$(g/cm$^3$) | 2.138 | 2.138 | 2.086 | 2.177 |
| | | | | |
| $2\theta$ range for data collection | ≤65.12 | ≤54.94 | ≤65.13 | ≤54.84 |
| No. of reflections collected | 4454 | 1978 | 4849 | 2356 |
| No. of independent reflections | 1192 | 747 | 1218 | 732 |
| No. of reflections with $I > 2\sigma(I)$ | 899 | 648 | 987 | 530 |
| No. of parameters refined | 64 | 62 | 64 | 64 |
| R(int) | 0.026 | | 0.024 | 0.068 |
| Final $R_1$, $wR_2$ factors [$I > 2\sigma(I)$] | 0.027, 0.061 | 0.026, 0.070 | 0.024, 0.062 | 0.046, 0.117 |
| Goodness-of-fit | 1.010 | | 1.064 | 1.118 |
| | | | | |
| Reference | (1) | (2) | (1) | (3) |

References: (1) This study; (2) Ye et al. (2010); (3) Yoneyama et al. (2013).

Table 2. Determined chemical compositions (in wt.%) for lazaraskeite-$M_1$ and lazaraskeite-$M_2$

| Constituent | lazaraskeite-$M_1$ (average of 6 analyses) | lazaraskeite-$M_2$ (average of 7 analyses) | Standard |
|---|---|---|---|
| Cu | 30.17(21) | 29.98(22) | Chalcopyrite $CuFeS_2$ |
| C | 22.6(2) | 22.2(2) | (1) |
| H | 2.84 | 2.83 | (2) |
| O | 45.23 | 44.94 | (2) |
| Total | 100.84 | 99.95 | |

Note:
(1): The C contents of 22.6(2) and 22.2(2) wt.% for lazaraskeite-$M_1$ and lazaraskeite-$M_2$, respectively, obtained from an Elemental Combustion System equipped with mass spectrometry, agree well with the ideal value of 22.49 wt.%. The determined $\delta^{13}C$ ‰ value is -37.7(1) for lazaraskeite-$M_1$ and -37.8(1) for lazaraskeite-$M_2$.
(2): The H and O contents were calculated based on the stoichiometry verified by the crystal structure determination.
(3): The electron microprobe analysis data points for the two polytypes were obtained from several crystals because they were easily damaged by the electron beam, even with the moving stage and large electron beam size.

Table 3a. Powder X-ray diffraction data of lazaraskeite-$M_1$.

| *I%* | $d_{meas}$ | $d_{cal}$ | *h* | *k* | *l* |
|---|---|---|---|---|---|
| **100** | **5.640** | **5.638** | **0** | **1** | **1** |
| **51.9** | **4.771** | **4.760** | **1** | **0** | **-1** |
| 2.5 | 4.324 | 4.335 | 0 | 2 | 0 |
| 21.1 | 4.252 | 4.258 | 1 | 1 | 0 |
| 10.9 | 3.747 | 3.743 | 0 | 2 | 1 |
| 15.2 | 3.627 | 3.630 | 1 | 0 | 1 |
| 8.2 | 3.417 | 3.412 | 0 | 1 | 2 |
| **63.2** | **3.344** | **3.348** | **1** | **1** | **1** |
| **25.2** | **3.230** | **3.227** | **1** | **1** | **-2** |
| 16.3 | 3.206 | 3.205 | 1 | 2 | -1 |
| 10.7 | 2.818 | 2.819 | 0 | 2 | 2 |
| 7.5 | 2.784 | 2.783 | 1 | 2 | 1 |
| 4.5 | 2.692 | 2.693 | 0 | 3 | 1 |
| 21.7 | 2.501 | 2.504 | 1 | 1 | 2 |
| 4.7 | 2.422 | 2.419 | 1 | 1 | -3 |
| 4.4 | 2.382 | 2.380 | 2 | 0 | -2 |
| 11.2 | 2.296 | 2.295 | 2 | 1 | -2 |
| **25.3** | **2.223** | **2.223** | **1** | **3** | **-2** |
| 11.5 | 2.179 | 2.178 | 1 | 2 | -3 |
| 4.8 | 2.125 | 2.129 | 2 | 2 | 0 |
| **22.2** | **2.086** | **2.086** | **2** | **2** | **-2** |
| 6.6 | 2.004 | 2.005 | 2 | 1 | -3 |
| 6 | 1.972 | 1.973 | 1 | 4 | -1 |
| 11.8 | 1.912 | 1.912 | 2 | 3 | -1 |
| 8 | 1.881 | 1.879 | 0 | 3 | 3 |
| 4.2 | 1.858 | 1.856 | 0 | 0 | 4 |
| 5 | 1.808 | 1.807 | 1 | 2 | 3 |
| 2.8 | 1.705 | 1.706 | 0 | 2 | 4 |
| 5.5 | 1.675 | 1.674 | 2 | 2 | 2 |
| 4.3 | 1.644 | 1.643 | 1 | 4 | -3 |
| 3 | 1.632 | 1.634 | 1 | 5 | 0 |
| 4.6 | 1.614 | 1.614 | 2 | 2 | -4 |
| 12 | 1.603 | 1.604 | 1 | 3 | -4 |
| 3.1 | 1.491 | 1.492 | 1 | 2 | 4 |
| 3.5 | 1.453 | 1.453 | 3 | 3 | -2 |
| 4.7 | 1.431 | 1.434 | 2 | 5 | -1 |
| 2.6 | 1.348 | 1.347 | 0 | 6 | 2 |

Table 3b. Powder X-ray diffraction data of lazaraskeite-$M_2$.

| $I$% | $d_{meas}$ | $d_{cal}$ | $h$ | $k$ | $l$ |
|---|---|---|---|---|---|
| **100.0** | **5.622** | **5.633** | **0** | **1** | **1** |
| **32.6** | **4.816** | **4.829** | **1** | **0** | **-1** |
| 4.6 | 4.313 | 4.323 | 0 | 0 | 2 |
| **22.5** | **4.190** | **4.203** | **1** | **1** | **0** |
| 1.9 | 4.042 | 4.056 | 1 | 0 | 1 |
| 5.1 | 3.727 | 3.736 | 0 | 1 | 2 |
| **30.2** | **3.550** | **3.560** | **1** | **1** | **1** |
| 1.5 | 3.410 | 3.411 | 0 | 2 | 1 |
| **20.4** | **3.289** | **3.293** | **1** | **1** | **-2** |
| 2.9 | 2.993 | 3.001 | 1 | 2 | 0 |
| 5.5 | 2.940 | 2.943 | 1 | 2 | -1 |
| 7.9 | 2.813 | 2.817 | 0 | 2 | 2 |
| 10.3 | 2.788 | 2.795 | 1 | 1 | 2 |
| **14.3** | **2.732** | **2.739** | **1** | **2** | **1** |
| 9.5 | 2.576 | 2.581 | 1 | 1 | -3 |
| 2.1 | 2.411 | 2.414 | 2 | 0 | -2 |
| 11.6 | 2.338 | 2.341 | 1 | 2 | 2 |
| 4.3 | 2.294 | 2.296 | 2 | 1 | -2 |
| **24.2** | **2.209** | **2.218** | **2** | **1** | **1** |
| 7.9 | 2.095 | 2.102 | 2 | 2 | 0 |
| 2.3 | 2.049 | 2.053 | 1 | 3 | -2 |
| 14.0 | 2.022 | 2.024 | 2 | 2 | -2 |
| 3.4 | 1.965 | 1.970 | 2 | 2 | 1 |
| 9.1 | 1.912 | 1.914 | 1 | 3 | 2 |
| 2.8 | 1.874 | 1.878 | 0 | 3 | 3 |
| 6.0 | 1.857 | 1.859 | 1 | 2 | -4 |
| 1.4 | 1.834 | 1.837 | 2 | 0 | -4 |
| 2.9 | 1.804 | 1.807 | 1 | 1 | 4 |
| 5.3 | 1.785 | 1.789 | 2 | 3 | -1 |
| 1.8 | 1.733 | 1.734 | 3 | 0 | -1 |
| 1.7 | 1.696 | 1.706 | 0 | 4 | 2 |
| 2.6 | 1.679 | 1.684 | 0 | 1 | 5 |
| 2.3 | 1.654 | 1.657 | 1 | 4 | -2 |
| 3.6 | 1.643 | 1.647 | 2 | 2 | -4 |
| 4.3 | 1.611 | 1.614 | 2 | 3 | -3 |
| 1.8 | 1.576 | 1.581 | 1 | 4 | 2 |
| 1.2 | 1.567 | 1.572 | 3 | 1 | 1 |

Table 4. Selected bond distances and angles in lazaraskeite.

| | Lazaraskeite form-1 (This study) | Lazaraskeite form-1 (Ye et al. 2010) | Lazaraskeite form-2 (This study) | Lazaraskeite form-2 at 150K (Yoneyama et al. 2013) |
|---|---|---|---|---|
| | Distance (Å) | Distance (Å) | Distance (Å) | Distance (Å) |
| Cu- O1 × 2 | 1.9199(12) | 1.920 | 1.9248(10) | 1.934(4) |
| -O2 × 2 | 1.9341(12) | 1.936 | 1.9634(11) | 1.959(4) |
| -O3 × 2 | 2.5423(12) | 2.546 | 2.4375(11) | 2.432(4) |
| Average | 2.1321 | 2.133 | 2.1085 | 2.109 |
| C1-O1 | 1.265(2) | 1.265 | 1.2623(18) | 1.261(6) |
| -O3 | 1.248(2) | 1.245 | 1.2506(17) | 1.248(6) |
| C1-C2 | 1.510(2) | 1.514 | 1.515(2) | 1.516(9) |
| C2-H2 | 0.92(3) | 0.91 | 0.98(3) | 0.97(6) |
| -H3 | 0.94(2) | 0.93 | 0.94(3) | 0.83(5) |
| -O2 | 1.415(2) | 1.421 | 1.4214(18) | 1.431(7) |
| O2-H1 | 0.71(3) | 0.76 | 0.93(2) | 0.78(7) |
| <O1-C1-O3 | 123.34(14)° | 123.38° | 123.45(13)° | 123.4(5)° |
| <O1-C1-C2 | 118.07(14)° | 118.10° | 118.77(13)° | 118.4(5)° |
| <O3-C1-C3 | 118.57(14)° | 118.51° | 118.53(13)° | 118.2(5)° |
| <O2-C2-C1 | 108.53(14)° | 108.48° | 108.80(12)° | 108.4(5)° |
| O2…O3 | 2.5821(17) | 2.579 | 2.5920(14) | 2.604(6) |
| <O2-H1…O3 | 172(3)° | 174.47° | 172(2)° | 167(4)° |

Table 5. Tentative assignments of major Raman bands for lazaraskeite

| Bands ($cm^{-1}$) | Assignment |
|---|---|
| 2760-3100 | C-H and O-H stretching vibrations. |
| 2230-2650 | O-H…O interaction. |
| 1200-1670 | C-O and C-C stretching vibrations in the $C_2H_3O_3^-$ glycolic group. |
| 840-1100 | C-OH stretching vibrations, as well as and O-C-O bending vibrations in $C_2H_3O_3^-$ glycolic group. |
| 400-800 | Cu-O stretching vibrations, H-C-H bending vibrations, and C-C-O bending vibrations in $C_2H_3O_3^-$ glycolic group. |
| <400 | Lattice and O-Cu-O bending vibrational modes. |

**Figure 1**


**Figure2**

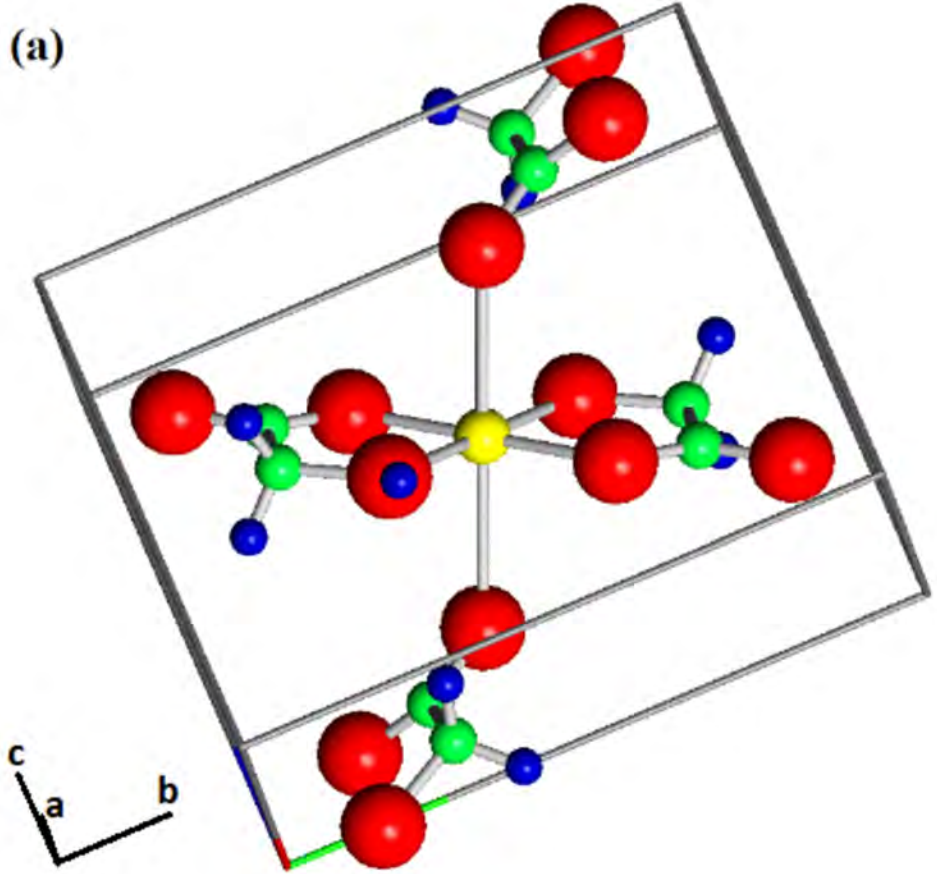


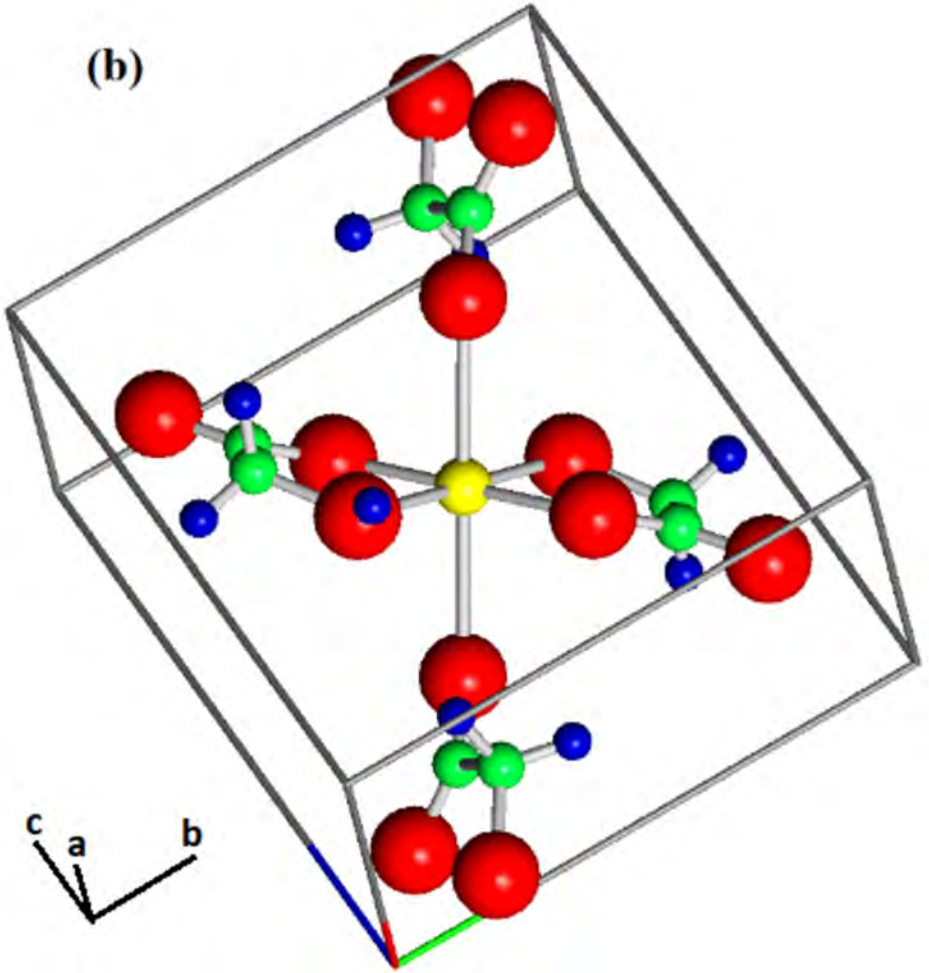


Figure 2

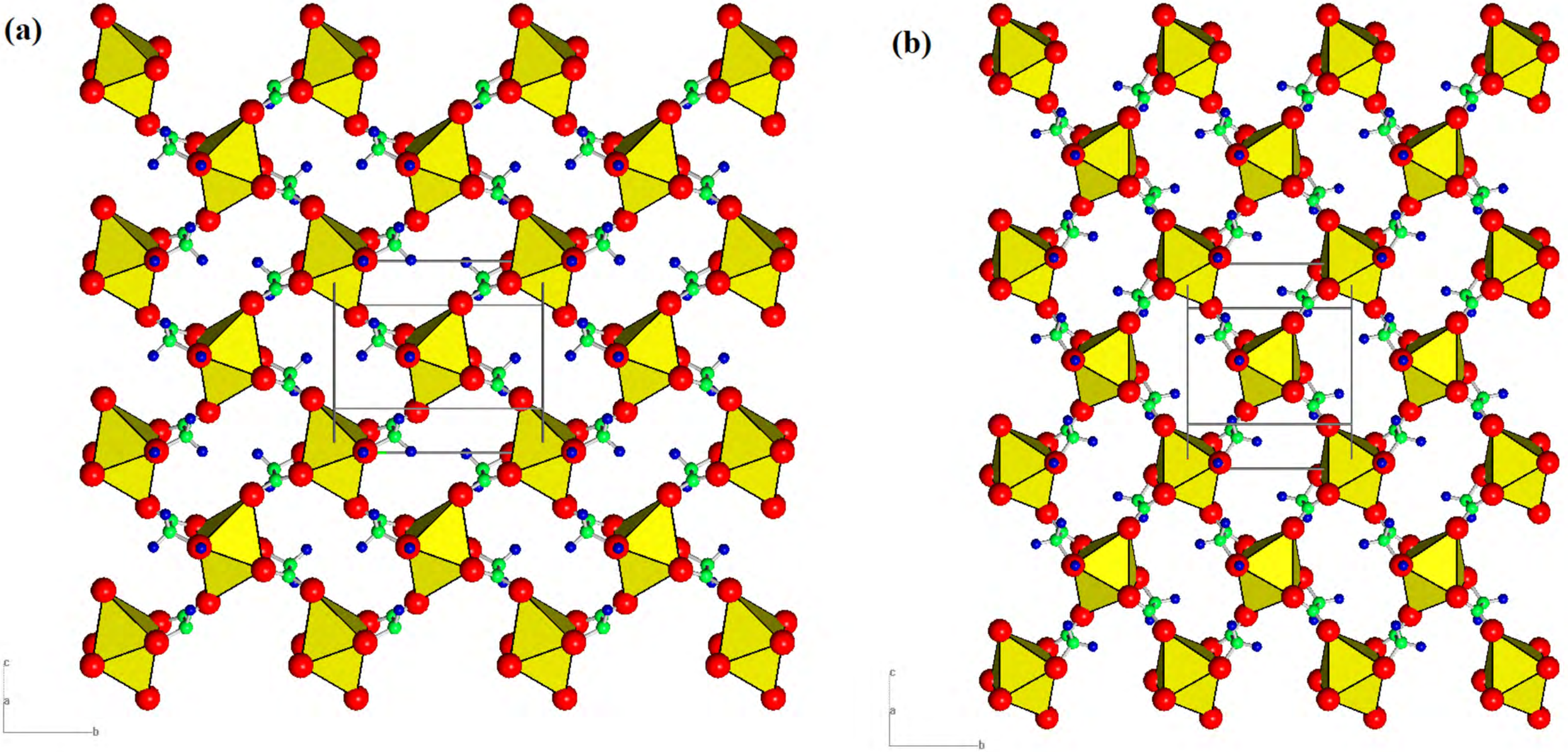


**Figure 4.**

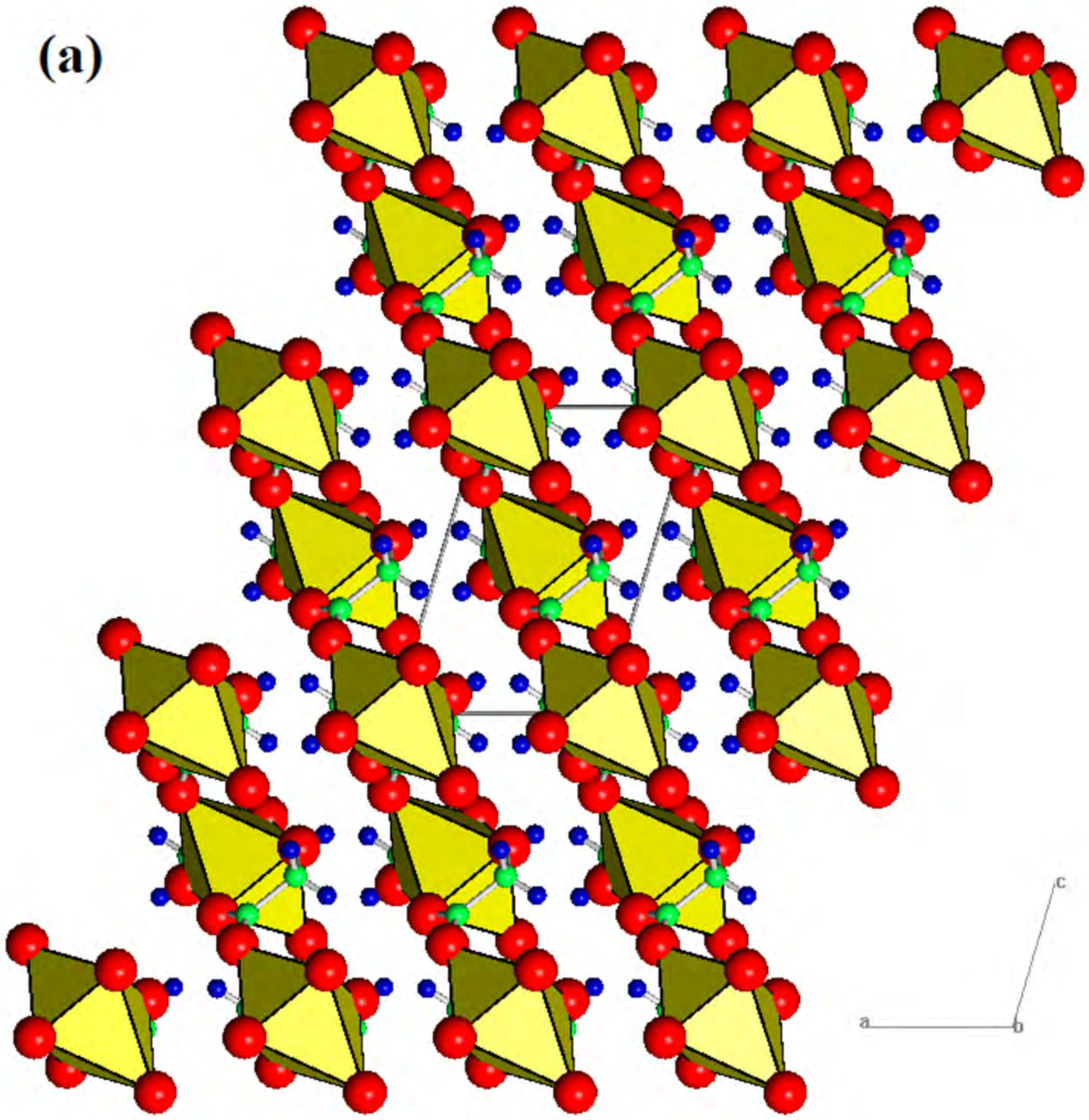


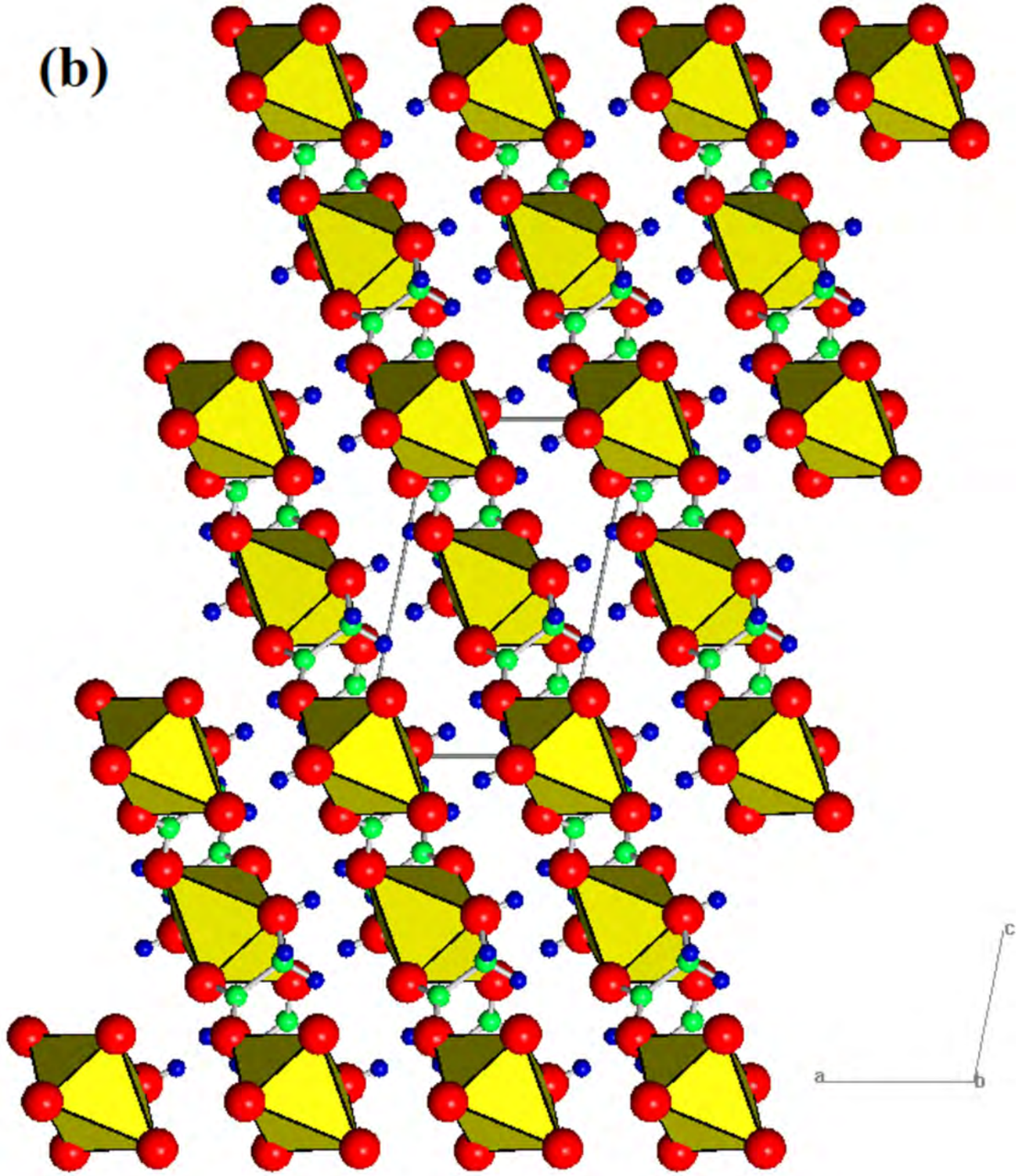


**Figure 5**

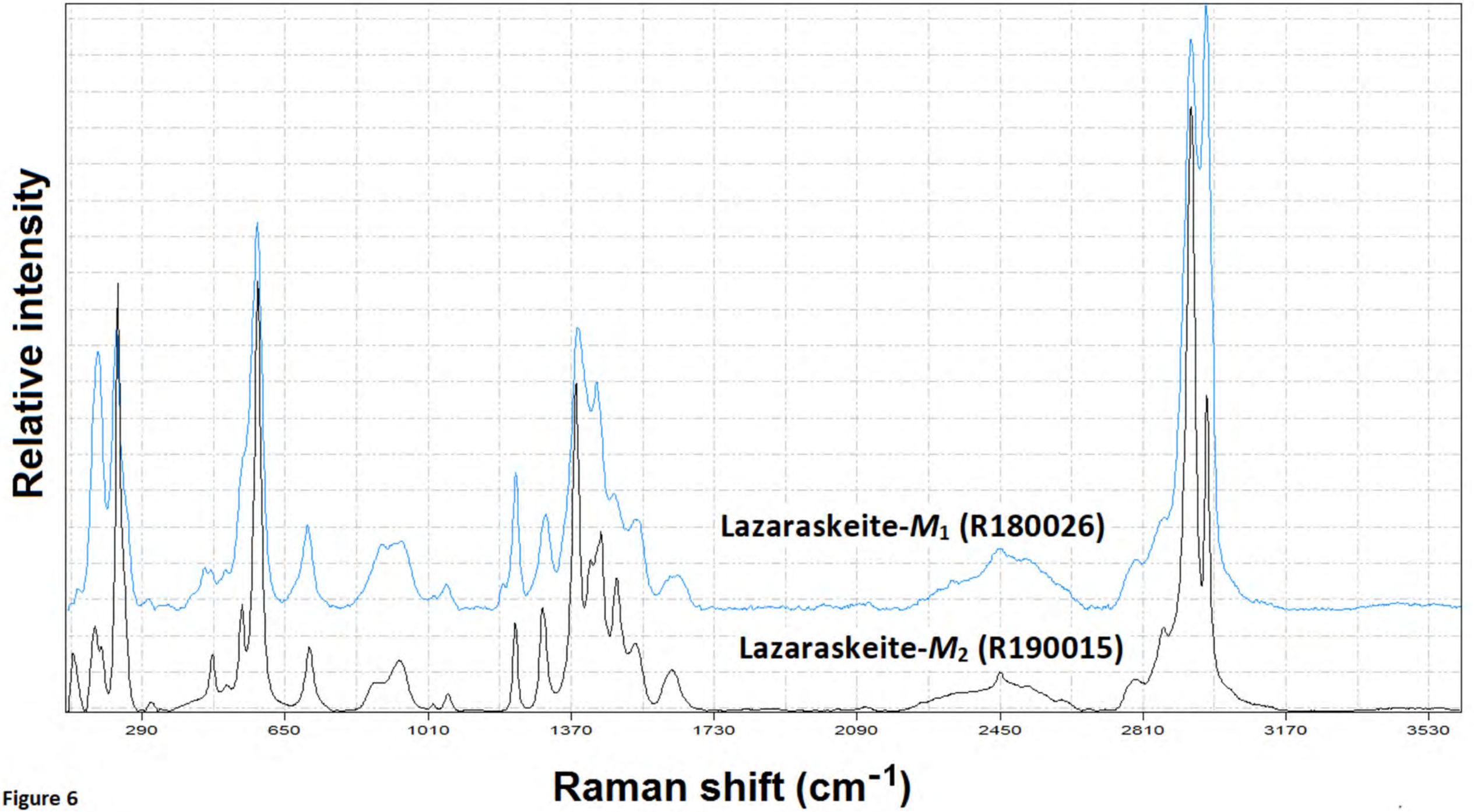
Relative intensity
Lazaraskeite-$M_1$ (R180026)
Lazaraskeite-$M_2$ (R190015)
290
650
1010
1370
1730
2090
2450
2810
3170
3530
Raman shift (cm$^{-1}$)

Figure 6